Tellus (1983), *35B*, 177–188

Some radiation budget and cloud measurements derived from Meteosat 1 data

By ROGER W. SAUNDERS[1] and GARRY E. HUNT[2], *Laboratory for Planetary Atmospheres, Department of Physics and Astronomy, University College London, London WC1E 6BT, England*

(Manuscript received August 4; in final form November 19, 1982)

ABSTRACT

Visible and infrared digitally encoded images from Meteosat 1 have been converted into broad band reflected and emitted irradiances in order to derive the radiation budget of the underlying surface/atmosphere. These fluxes were determined once an hour over Western Europe for August 21, 1978, averaged over a 1° lat/long grid. This has allowed a daily mean to be calculated from the twenty-four observations and a standard deviation, a measure of the diurnal variability of the albedo and emitted irradiance. In addition, cloud amounts at three levels were derived every hour. The algorithms developed could in principle be applied to determining radiation budget and cloud parameters in real time from geostationary data, allowing an archive of satellite derived data to be collected.

1. Introduction

The importance of the Earth's radiation budget in determining climate has long been recognized. With the advent of satellites, a platform is now available outside the atmosphere from which meteorologically useful continuous measurements of the Earth's radiation budget can be made, at least in principle (Vonder Haar and Suomi, 1971; Gruber and Winston, 1978; Stephens et al., 1981). Any changes in radiative balance may be indicative of changes in the general circulation pattern so that both should be studied in parallel.

Radiometers on meteorological satellites monitor the reflected solar and emitted terrestrial radiance in narrow spectral intervals (0.4–1.1 microns VIS, and 10.5–12.5 microns IR over a variety of nadir angles for Meteosat). One of the main problems is to convert these narrow spectral interval radiances into total reflected and emitted fluxes integrated over all wavelengths and solid angles.

Reflected and emitted radiances can, under certain conditions, be used to determine if cloud is present within the field of view of the radiometer and, if so, the height of its top. The combination of measured reflected and emitted irradiances and cloud amounts and types averaged over a suitable grid size and time period is useful for numerical prediction models both as input and as a more suitable output to compare the satellite observations with predictions, although as Hunt (1982) has shown, accurate estimates of cloud thickness remain a further problem. This paper describes a method developed at UCL on the Interactive Planetary Image Processing System (IPIPS—Hunt et al., 1982) which converts the raw satellite counts into climatological parameters averaged over a 1° lat/long grid once an hour. We provide an estimate of the statistical properties of the radiation budget and cloud parameters applied to the European sector for August 21, 1978.

2. Methodology

2.1. *Remapping of pixels*

The overall scheme for converting the raw radiance counts transmitted by Meteosat into reflected and emitted irradiances at the top of the atmosphere is shown in Fig. 1. The first problem is to "navigate" the input images so that individual pixels can be assigned a particular latitude and

[1] Present address: ESOC, Darmstadt, F.R. Germany.

[2] Present address: Atmospheric Physics Group, Imperial College, London SW7, England.

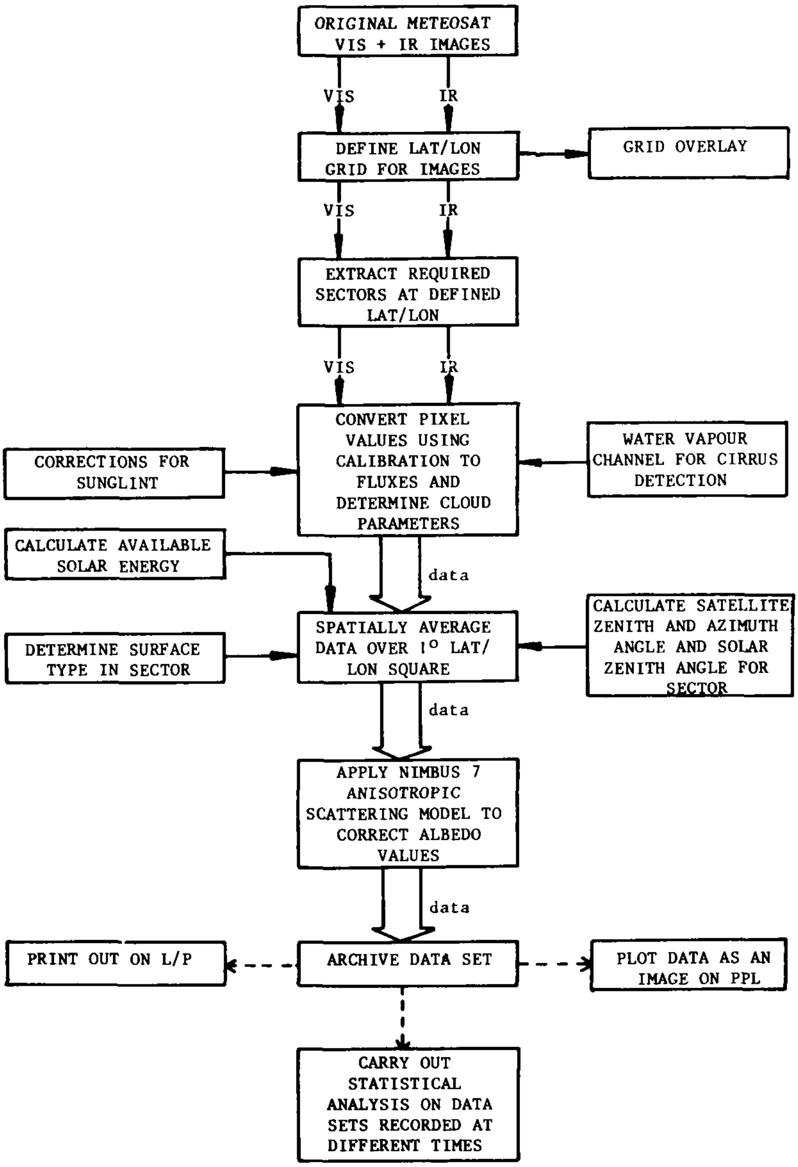

Fig. 1. The flow diagram for obtaining the radiation budget parameters from the raw satellite image data.

longitude. The pixel size used in this study corresponds to the Meteosat infrared pixel, which is 5 km square at the sub-satellite point. The visible pixels were spatially averaged to match the infrared pixels. With geostationary images there are two primary factors which affect navigation (Jones, 1981).

The orientation of the satellite can vary causing the image of the Earth's disc to shift relative to previous images. This effect can be removed by measuring the number of pixels from the top of the scan to the centre of the disc n_V and from the side of the scan to the centre n_H. Any shifts in the position of the disc will be measured by changes in n_V and n_H. These measurements can be made by applying an edge-detection process to the infrared full disc (2500 × 2500 pixel) image.

The other factor is that the actual position of the satellite wanders away from its nominal 0° lat/long position. This causes the viewpoint of the satellite to change so that the land masses move slightly with respect to the edge of the observed disc. Corrections could be computed from accurate satellite positions obtainable from the European Space Operations Centre (ESOC) at Darmstadt. However, a method was developed to infer this information by measuring the coordinates of a cloud-free landmark whose latitude and longitude are accurately known. Initially, the satellite is assumed to be at 0° lat/long ($SLA = 0$, $SLO = 0$); the pixel coordinates (L, S—line, sample) of the landmark at $X°$ latitude (north positive) and $Y°$ longitude (east positive) are given by

$$S = n_H \pm \frac{26.91 \times 10^7 \cdot R \cdot K \cdot \cos(\sin^{-1}(\sin(X)/K))}{(4.22 \times 10^4 - 6371 \cdot \gamma)6445} \quad \begin{matrix} \text{for } Y < 0 \\ \text{for } Y > 0 \end{matrix} \tag{2.1}$$

$$L = n_V - \frac{26.91 \times 10^7 \cdot R \cdot K \cdot \sin(x)/K}{(4.22 \times 10^4 - 6371 \cdot \gamma)6445} \tag{2.2}$$

where $\gamma = \cos(X + SLA)\cos(Y - SLO)$,
$K = \sin(\cos^{-1}(\gamma))$,

and R is the observed equatorial radius of the Earth in pixels.

If the calculated coordinates (L, S) do not coincide with the measured coordinates, then SLA and SLO are incremented by a small amount and a new set of coordinates is calculated. This iteration continues about 0° lat/long until the differences between the calculated and known coordinates are minimized to <1 pixel. The calculated values for SLA and SLO inserted in eqs. (2.1) and (2.2) may now be applied to all pixels whose field of view is on the Earth's surface. This method gave a positional accuracy of ± 2 pixels (10 km) over the European sector.

From the derived relationship between pixel coordinates and Earth coordinates, a 1° lat/long grid was defined over the Western European area from 34° N–58° N, 8° W–20° E. Each grid square contained approximately 300 pixels, although this number decreased for the most northerly latitudes. Since a variety of different grid sizes are being used in numerical models and in the analysis of spatially averaged satellite datasets (Brooks, 1981), the algorithm has been made sufficiently flexible to allow for the data to be averaged over any required grid size.

2.2. *Calibration of radiometers*

The calibration of the Meteosat 1 VIS and IR channels involved converting the received digital counts or grey levels to observed radiances within a known spectral band through the use of calibration factors. These factors were obtained by comparing Meteosat counts with coincident ground data.

For the visible (VIS) channel, the factors given by Kriebel (1981), which convert VIS counts to radiance between 0.4 and 1.1 μm, were used. These were derived by high flying aircraft radiance measurements with the same filter limits as Meteosat, over uniform surfaces covering at least one simultaneously observed pixel. The factors vary with the underlying surface type because the reflectivity of different surfaces or clouds varies with frequency in different ways. For instance, cloud-free desert reflects all visible frequencies equally, whereas cloud-free ocean reflects higher frequencies more than lower frequencies. This has the effect of altering the conversion factor from the counts measured within the finite spectral band width of the Meteosat 1 VIS channel to the total radiance between 0.4 and 1.1 microns. The underlying surface type, m, was divided into land, ocean or cloud. It is known whether a pixel is over land or ocean from its latitude and longitude so the problem is to determine the fractional cloud cover within each pixel. This value is determined by a threshold scheme applied to each pixel, set to detect cloud at the 50% level. The threshold was determined empirically from a few test cases and is a function of the solar zenith angle. The method used both VIS and IR counts to test for the presence of cloud. The appropriate factor, k_m, then gave the total reflected radiance (n_r) between 0.4 and 1.1 microns for model type m.

$$n_r = k_m C_{VIS} \text{ W m}^{-2} \text{ str}^{-1} \tag{2.3}$$

where C_{VIS} is the Meteosat visible channel count.

The Meteosat infrared channel has been calibrated by various authors. ESA (Morgan 1980) and Köpke (1980) derive a conversion factor, k, which gives the emitted radiance, n_e, within the filter profiles (10.5–12.5 microns)

$$n_e = k\cdot(C_{IR} - 2.5)\ \mathrm{W\ m^{-2}\ str^{-1}} \quad (2.4)$$

where C_{IR} is the Meteosat infrared channel count.

The factor k was derived by a comparison of sea surface temperature measurements in the North Sea, Mediterranean Sea and Red Sea with IR counts from simultaneously observed cloud-free pixels. Another technique using the moon as a calibration source (Antikidis and Reynolds, 1979) has also been investigated and gives good agreement with the previous method.

2.3. *Conversion to unfiltered radiances*

For the reflected visible radiance, the conversion to an albedo, A_u, over all wavelengths was derived by assuming that the albedo between the Meteosat VIS filter band limits (0.4–1.1 μm) was identical. This assumption was checked by comparing the derived Meteosat reflected radiance (integrated over all wavelengths) with the Nimbus 7 ERB total reflected radiance (Saunders et al., 1983). No overall bias between the two sets of measurements was found. The first step is to convert to unfiltered radiance N_r using the relation:

$$N_r = \frac{A_f S \cos\psi(t) f}{\pi} = \frac{n_r S}{s}\ \mathrm{W\ m^{-2}\ str^{-1}} \quad (2.5)$$

since the filtered diffuse albedo is given by

$$A_f = \frac{\pi n_r}{s\cdot\cos\psi(t) f} \quad (2.6)$$

where

- N_r is the unfiltered reflected radiance
- n_r is the filtered reflected radiance
- S is the unfiltered solar constant 1376 W m^{-2} at 1 AU (Hickey et al., 1980)
- s is the filtered solar constant between 0.4 and 1.1 μm 900.9 W m^{-2} (Thekaekara and Drummond, 1971)
- f is a correction factor from 1 AU to be applied to the solar constant due to variations in the Earth–Sun distance
- $\psi(t)$ is the solar zenith angle for the grid centre at time t.

The mean unfiltered radiance is calculated for each grid square together with the populations of pixels assigned to cloud, land or ocean. The mean satellite zenith angle, θ, solar zenith angle, ψ, and relative azimuth angle, ϕ, (between sun and satellite) were also calculated for the centre of the grid area. Gube (1982) suggested that the anisotropic scattering effects may be accounted for by a radiative transfer model. This approach is limited by the ability to represent the processes involved. We have therefore adopted a more realistic approach. To allow for anisotropic scattering effects, the Nimbus 7 ERB data of Stowe et al. (1980), which gives angular scattering models for four different surface types—land, ocean, snow and cloud—was used. Values of the anisotropic factors are given for ten different solar zenith angle ranges. The average irradiance of reflected radiation for model type, m, is given by:

$$W_{r,m} = \frac{N_{r,m}(\theta,\phi,\psi)}{a_m(\theta,\phi,\psi)}\ \mathrm{W\ m^{-2}} \quad (2.7)$$

where a_m is the anisotropic factor for model m (greater than 1 means the surface reflects more than an isotropic surface of the same albedo).

The instantaneous albedo, A averaged over one grid square, is now given by

$$A = \frac{1}{S\cos\psi(t) f}\,\frac{\sum_{m=1}^{3} W_{r,m} P_m}{\sum_{m=1}^{3} P_m} \quad (2.8)$$

where P_m is the population of pixels of model type m in the grid square.

The emitted radiance measured by the Meteosat IR channel was converted to unfiltered irradiance following the procedure adopted by Gube (1980, 1982). The first regression relationship allows for limb darkening effects and is a function of which model atmosphere profile was used and so varies with latitude and season. Having converted the observed radiance to a nadir viewing angle of zero, a second regression relationship then converts this filtered radiance to unfiltered instantaneous irradiance W_e.

2.4. *Spatial and temporal averaging*

The parameters were archived for each 1° lat/long square so that the dataset produced was independent of the Meteosat projection. This is important since this dataset can then be easily interfaced with numerical models of the atmosphere which may predict some of the values measured here, for example, Slingo (1982), or can be compared with similar data derived from other satellites. The original satellite data is greatly compressed during this averaging process but the useful climatological information is retained. For a 1° lat/long area the original images (VIS + IR) can consist of up to 600 8-bit bytes, but this is reduced to less than twenty real numbers in the final dataset.

All pixels within each 1° lat/long grid square contributed to the mean values of reflected and emitted irradiance for that grid square. Values of standard deviation about the mean were also computed for each grid square and this gave an idea of the spatial variability of the parameter. The instantaneous values of each grid square were calculated once every hour from the Meteosat data. The emitted irradiances for each hour were averaged in the normal way to give a daily mean. However, to obtain a daily mean albedo which can only be measured during the daytime, the following procedure was adopted. The daily mean reflected irradiance $\overline{W}_r$ is given by

$$\overline{W}_r = \frac{1}{24} \sum_{i=1}^{24} W_{r,i} \tag{2.9}$$

where $W_{r,i}$ is the instantaneous reflected irradiance for hour i, which would be zero at night.

The daily mean albedo $\bar{A}$ can then be expressed by

$$\bar{A} = \frac{W_r}{Sf \cos \overline{\psi(t)}} = \sum_{i=1}^{24} A_i \left(\frac{\cos \psi(t_i)}{\sum_{i=1}^{24} \cos \psi(t_i)} \right) \tag{2.10}$$

where the denominator in the first expression is the mean solar insolation for the day of interest. It should be emphasized that this results in a different mean albedo to that which is obtained by averaging together instantaneous albedos. This latter average albedo would be a measure of the daily mean reflectivity of the Earth's surface and atmosphere, whereas the mean albedo defined in eq. (2.10) is a measure of the daily mean radiation reflected back to space by the Earth's surface and atmosphere which is the quantity of interest.

The standard deviation about the mean was also calculated and this gave a measure of the diurnal variability for each parameter. In the case of the albedo the standard deviation is given by

$$A_{SD} = \sqrt{\sum_{i=1}^{24} \left(\left[\frac{A_i \cdot \cos \psi(t_i)}{\sum_{i=1}^{24} \cos \psi(t_i)} \right]^2 - \bar{A}^2 \right)} \tag{2.11}$$

2.5. *Derivation of cloud amounts*

Cloud amounts and cloud top heights were derived from the Meteosat VIS and IR data by an automated decision process summarized in Table 1. This consisted of using information from both channels (when available) and applying predefined threshold radiances to make the decision as to whether a pixel was assigned to be cloudy or cloud free and also what cloud top height the cloudy pixels were assigned.

Table 1. *Cloud classification scheme*

Cloud type (1)	Albedo threshold (2)	Infrared radiance† thresholds for different models: Mid-lat summer	Mid-lat spring/autumn	Mid-lat winter	Tropical
Low <2 km cloud top height	>50%	>64 W m^{-2}	>55 W m^{-2}	>47 W m^{-2}	>67 W m^{-2}
Medium 2–6 or 7 km* cloud top height	>50%	38–64 W m^{-2}	35–55 W m^{-2}	31–47 W m^{-2}	40–67 W m^{-2}
Deep convection or frontal >6 or 7 cm* cloud top height	>50%	<38 W m^{-2}	<35 W m^{-2}	<31 W m^{-2}	<40 W m^{-2}
Cirrus >6 or 7 km* cloud top height	⩽50%	<38 W m^{-2}	<35 W m^{-2}	<31 W m^{-2}	<40 W m^{-2}

(1) From International Cloud Atlas Vol. 1, WMO 1956.
(2) From WMO Tech Note 124, p. 1.
* 6 km at midlatitudes, 7 km at tropical latitudes (<30°).
† Radiance is that measured within the Meteosat filter profile corrected for limb darkening.

There are several problems associated with cloud detection schemes using visible and infrared wavelengths. Low cloud at night is normally difficult to distinguish from cloud-free conditions because of the small magnitude of the temperature difference between the ocean or land surface and the cloud top. Reflected radiances at visible wavelengths are one effective means of detecting low cloud. Over snow/ice, the situation becomes more difficult as even reflected radiances cannot easily discriminate between cloud and surface. However, there is evidence (Knottenberg and Raschke, 1982) that the 3.7 micron channel of the AVHRR on the NOAA meteorological satellites is able to improve the discrimination between clouds and snow/ice. Another area of difficulty is the detection of thin cirrus cloud. The 11 micron IR channel is more sensitive to cirrus cloud than the visible channel. However, by inspection of Meteosat images at both 11 microns (IR) and 6.3 microns (WV), the latter wavelength appears to be a better discriminator between cloud free areas and regions of thin cirrus. Finally, over the ocean in regions where sunglint is apparent in the satellite images or when high concentrations of aerosols are present due to volcanic activity, cloud detection from the reflected radiance is rendered much more difficult as simple threshold methods will not apply. In spite of the limitations, the information that these cloud parameters provide is essential to support the radiation budget analyses described in this paper.

3. Results for August 21, 1978

In this section, we describe the results of a study using one complete day of hourly Meteosat data over Western Europe, to test the spatial and temporal averaging algorithms, and compare them with other recently published results. Hourly data for August 21, 1978, were analysed by the procedures described in the previous section. To illustrate an instantaneous measurement, Fig. 2 shows the VIS 2(A) and IR 2(B) images for 11.45 GMT in a square lat/long projection, together with values of the albedo and emitted irradiance represented as grey shades which relate to albedos or emitted irradiances. The values are only displayed in steps of 10% (albedo) and 17.5 W m^{-2} (emitted irradiance) although the actual digital values are archived to accuracies of 0.1% and 0.1 W m^{-2} respectively. Each square in Figs. 2c and 2d is 1° lat/long.

The albedos of the cloud-free land appear to be around 20% whereas the sea was less than 10%. Low and high clouds increased the albedo to 40–60% when averaged over a 1° lat/long grid. These results can be compared with Gube (1982) where albedos of 20–30% are reported for land and 10% for sea.

Emitted irradiances in Fig. 2d were greater than 285 W m^{-2} over cloud-free land; the values over the Mediterranean were about 285 W m^{-2}, whereas low cloud reduced the values to 250 W m^{-2} and high cloud to below 200 W m^{-2}. This was in good agreement with measurements made over Africa also using Meteosat (Gube, 1980) where land had emitted irradiances greater than 280 W m^{-2}, sea surface 260–280 W m^{-2} and high cloud 150–200 W m^{-2}.

Results, such as those shown in Figs. 2c and 2d were produced for every hour of the day (from midnight to midnight) and while they form the basis of the extended analysis they may also be used to produce a time lapse sequence to display pictorially the variation in the derived radiation budget. This allows the diurnal variability in radiation budget parameters (Saunders and Hunt, 1980, Gube, 1980, 1982) to be studied over many different surface/cloud types.

Figs. 3a and 3b show the daily means computed from the hourly data as described in Section 2.4. The higher albedos due to cloud are averaged over the day giving intermediate values between cloud-free and complete cloud cover. Areas where intense cumulonimbus clouds developed (Ward et al., 1983) alter the mean albedo by 5% and the mean emitted irradiances by 30 W m^{-2}. This compared favourably with a change of 35 W m^{-2} in emitted irradiance over enhanced tropical convection measured by Smith (1980) using SMS 1 data. The daily mean emitted irradiance over the land and adjacent sea are the same and decreased from 290 to 250 W m^{-2} with increasing latitude (34° N to 58° N). This is slightly higher than the zonal mean irradiance values reported by Stephens et al. (1981) from Nimbus 6 data because the European area was unusually cloud free on the 21st day of August 1978.

In Figs. 3c and 3d we show the standard deviation about the daily mean of the computed

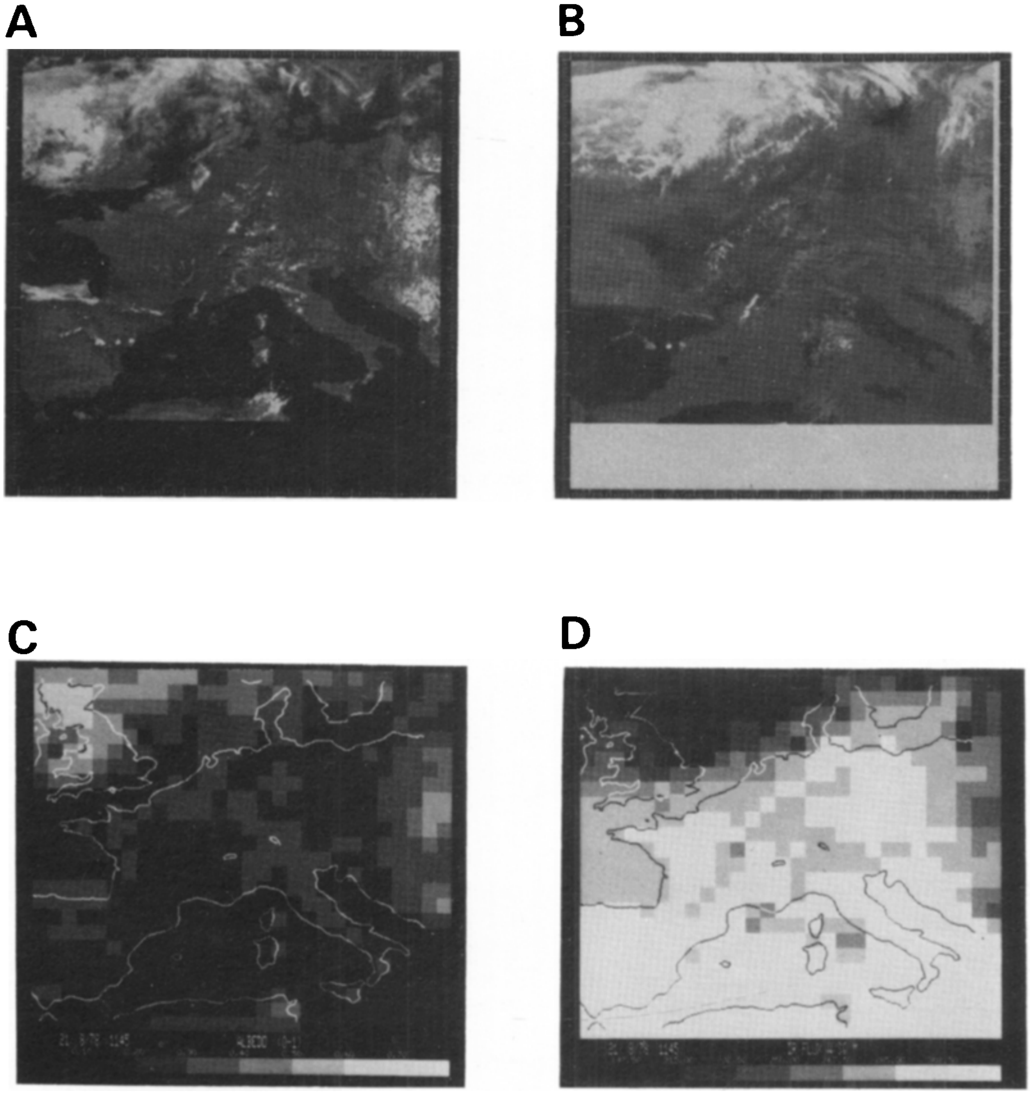

Fig. 2. Visible (a) and infrared (b) square projections of Europe from Meteosat and the albedo (c) and outgoing flux (d) averaged over 1° lat/long squares, derived from the VIS and IR satellite images for 11.45 GMT on August 21, 1978. The parameter values are shown on the grey scale at the bottom.

albedo and emitted radiances, which should be compared with estimated relative errors of ~2% in albedo and ±2 W m^{-2} in the emitted radiation. Both albedos and emitted irradiance have relatively high standard deviations of 6% and 8 W m^{-2} where cloud has formed or dissipated, such as over Northern France, Northern Spain and North Western Britain. In particular, the cumulonimbus clouds over the Pyrenees and south-east coast of Spain show up as a large standard deviation of 9 W m^{-2} in the emitted irradiance. The diurnal variability of emitted irradiance over cloud-free land is well shown in 3d, where the land has a higher standard deviation of 2–3 W m^{-2} compared with 0.3 W m^{-2} for the surrounding ocean.

High values of standard deviation are areas where polar orbiting satellites, such as Tiros-N and Nimbus 7, which only observe a particular location

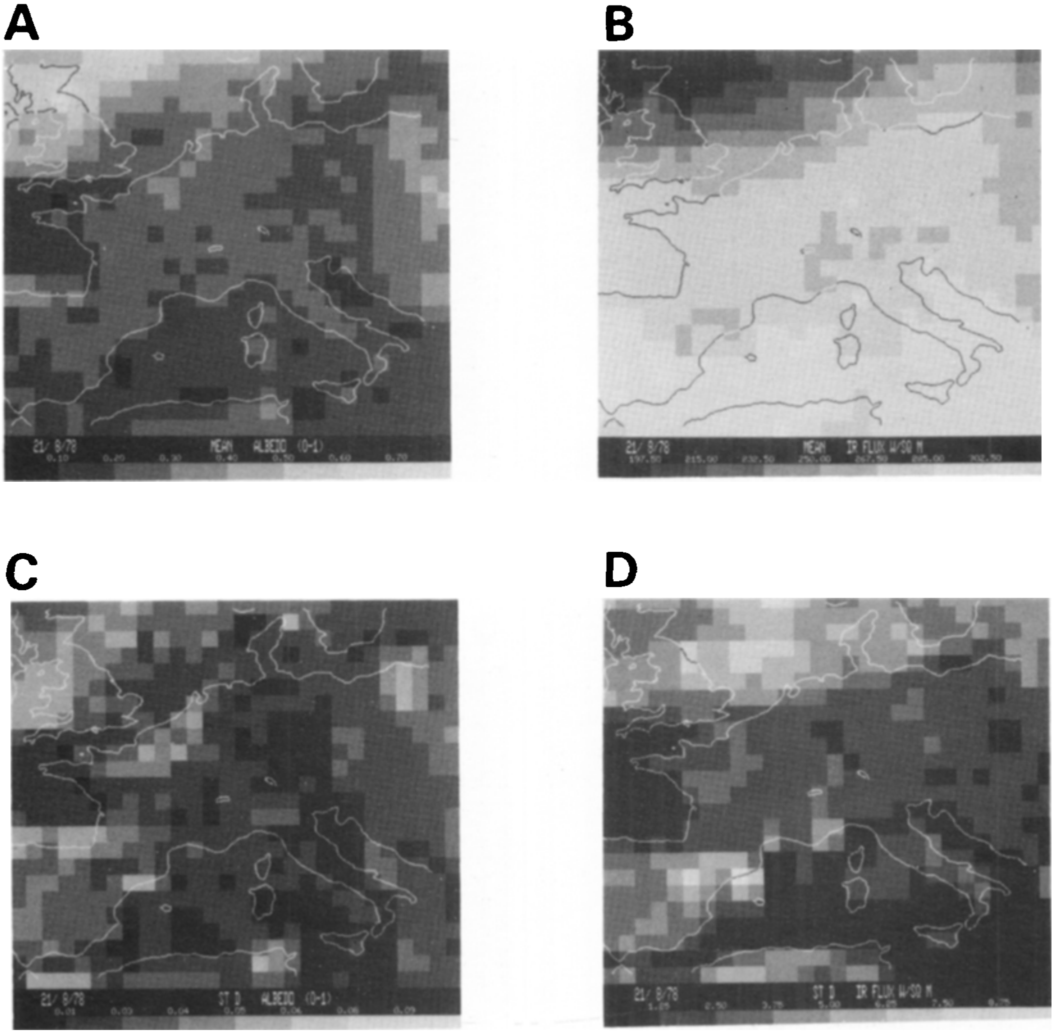

Fig. 3. The mean albedo (a) and longwave flux (b) for August 21, 1978, over W. Europe and their standard deviations for that day (c and d).

twice a day, may have large errors in their daily means due to insufficient diurnal sampling (Saunders et al., 1983).

Using this European dataset, the following algorithms were developed to obtain a daily mean albedo and emitted irradiance from one albedo or two emitted irradiance polar orbiter observations.

Over cloud-free land, the albedo remains fairly constant, as shown in Fig. 3, so that to determine the daily mean we assume that the one daylight observation, $W_{r,p}$, is representative of the daily mean albedo $\bar{A}$.

$$\bar{A} = \frac{1}{nSf} \frac{\sum_{i=1}^{n} W_{r,i}}{\sum_{i=1}^{n} \cos Z_i} \sim \frac{W_{r,p}}{S \cdot f \cdot \cos Z_p} \qquad (3.1)$$

Daily mean	Meteosat observations	Polar orbiter observations

where

$W_{r,i}$ is the reflected irradiance for the ith hour observed by Meteosat

$W_{r,p}$ is the reflected irradiance measured by a polar orbiting satellite for a solar zenith angle Z_p

n is the number of Meteosat observations for that day.

The emitted irradiance varies considerably during the day over cloud-free areas, as shown in Fig. 3. Assuming two observations, W_{EN} (night-time flux) and W_{ED} (day-time flux) from a polar orbiter, the following relationship was found to give good diurnal means:

$$\overline{W_E} = \frac{1}{n}\sum_{i=1}^{n} W_{E,i} \sim \frac{W_{ED} - W_{EN}}{\cos(Z_D)}\overline{\cos(Z)} + W_{EN}. \quad (3.2)$$

Daily mean	Meteosat observations	Polar orbiter observations

where

$\overline{\cos(Z)}$ is the mean daily solar zenith angle

Z_D is the solar zenith angle an hour before the daytime observation (the hour's difference is due to thermal inertia).

Over cloud-free ocean, the albedo (corrected for anisotropic effects (i.e. sunglint)) is essentially constant so that eq. (3.1) can still be used. The emitted irradiance is virtually constant over the sea so that in this case eq. (3.2) can be simplified to:

$$\overline{W_E} = \frac{1}{n}\sum_{i=1}^{n} W_{E,i} \sim \frac{W_{ED} + W_{EN}}{2} \quad (3.3)$$

Daily mean	Meteosat observations	Polar orbiter observations

Over cloud, both albedo and emitted irradiance are dependent on cloud amount and height during the day. It is difficult to formulate a universal diurnal model for cloudiness, especially at mid-latitudes where synoptic features are not a function of the local time of day. Over the tropics, there is obviously a predictable diurnal cycle for the cumulonimbus cloud, and recent work by Minnis and Harrison (1981) and Gube (1980) has shown tht many other types of cloud also have diurnal cycles.

Kandel and Bézanger (1980) have used GOES-East IR data to study diurnal variations and observe that in some cases the minimum cloudiness over the ocean occurs in the afternoon, whereas in others the minimum cloudiness is in the early morning.

The derivation of cloud amounts for August 21, 1978, is shown in Fig. 4. The instantaneous values for the 11.45 GMT Meteosat observation averaged over a 2° lat/long grid are displayed together with the corresponding visible channel image in the same geometric projection. This allows a direct comparison between the original satellite image and the derived cloud amounts. The "low cloud" amounts in Fig. 4b show the low stratus "hugging" the north Spanish coast, and the scattered cumulus cloud over northern France, northern Italy and Tunisia. Significant medium height cloud amounts in Fig. 4c are shown to be associated with the edge of the frontal cloud over the north-west of England and with stratocumulus over large areas of eastern Europe. High cloud is assigned only to the intense frontal cloud passing over the North Sea and Scotland. Daily means and standard deviations for each class of cloud can be calculated from this dataset.

4. Conclusions

The case study presented here for August 21, 1978, has demonstrated the feasibility of obtaining albedos, emitted irradiances and cloud amounts for different cloud types from hourly Meteosat data. Uncertainties due to radiometer calibration, anisotropic scattering and the assumption that the albedo over the Meteosat filter profile is the same as the broad band albedo leads to a 10% uncertainty in the absolute albedo value. The relative error is 2%. For the emitted irradiance, uncertainties due to radiometer calibration and the inference of a broad band radiance from a narrow band radiance leads to an uncertainty of ± 10 W m^{-2} in the absolute value, while the relative error is ± 2 W m^{-2}. Evidence for the magnitude of these uncertainties can be obtained by comparing the Metosat values with values from other polar orbiting satellites viewing the same scene at the same time (Saunders et al., 1983). Errors in the daily mean values estimated from polar orbiters due to incomplete diurnal sampling can be much greater than the geostationary measurement uncertainties listed above. For instance, over the Netherlands a daily mean albedo of 0.35 is computed from the hourly data, whereas one polar orbiter measurement at a local time of 12.00 gave a value of 0.29. Similarly, for emitted irradiances over cloud-free land a daily

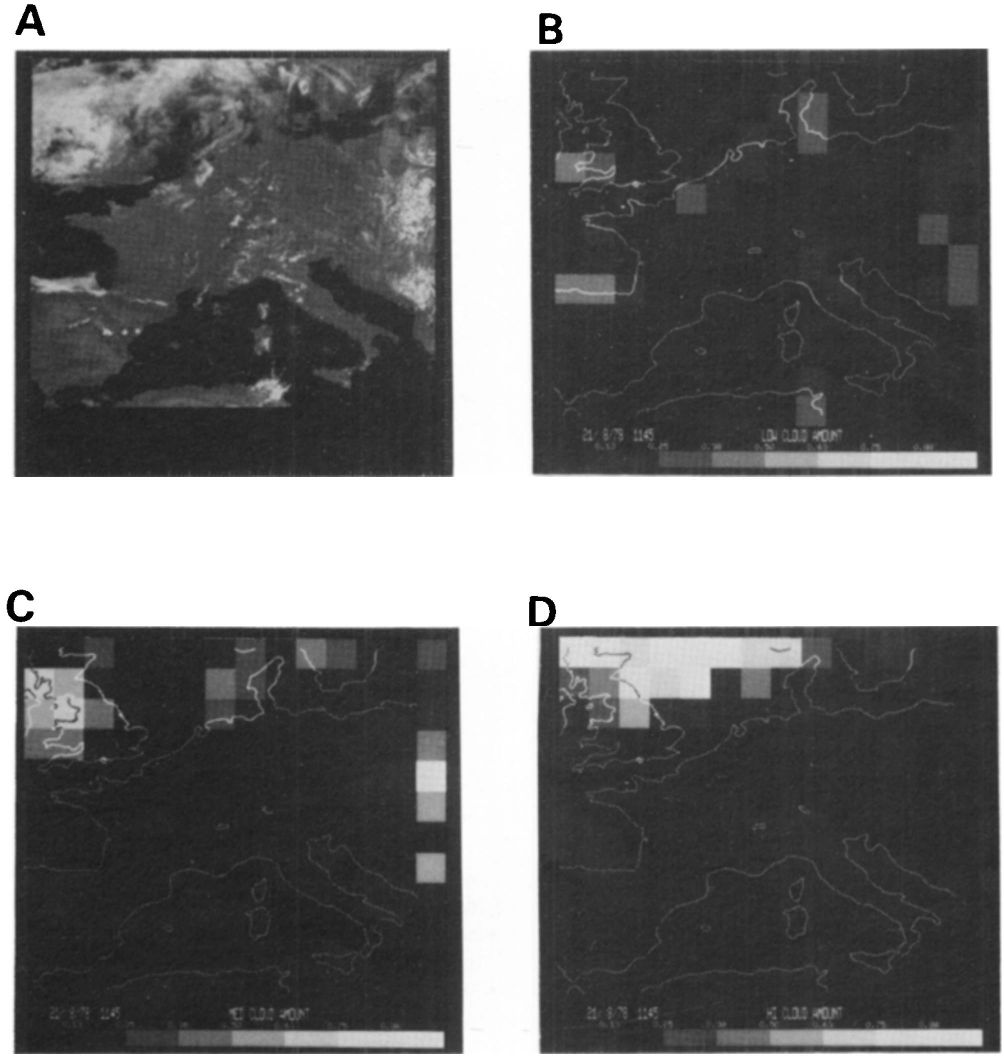

Fig. 4. Visible (a) square projection and low cloud (b), medium cloud (c) and high cloud amounts (d) averaged over 2° lat/long squares derived from the VIS and IR satellite images for 11.45 GMT on August 21, 1978. The minimum cloud amount shown in this plot is 10%. The actual data records cloud amounts down to 1%.

mean value of 302 W m^{-2} was obtained over central Spain whereas one polar orbiter at 12.00 LT would record a value of 327 W m^{-2}. Minnis and Harrison (1981) also give examples of the discrepancies between the 12.00 LT and the daily mean value over cloud and conclude that diurnal variations are significant. Uncertainties in cloud amounts were more difficult to estimate, but for the 2° lat/long squares shown in Fig. 4 an accuracy of $\pm 10\%$ in cloud cover is thought to be realistic for the multispectral threshold technique used. Of course, the relative uncertainties are much smaller than the values stated above, allowing smaller variations with respect to time or location to be seen.

The hourly data allow accurate daily means to be calculated (Saunders and Hunt, 1980). The diurnal variations about the mean were found to be significant for albedos and emitted irradiances where cloud had formed, dissipated or passed through the grid square. Cumulonimbus clouds caused the largest diurnal variations in emitted irradiances due to their large rate of change with time. Cloud-free land also produced a marked diurnal variation in the emitted irradiance. These variations have to be allowed for when calculating daily mean values from polar orbiter data which only make observations over a particular location twice a day.

Saunders et al. (1983) have shown, through the use of simultaneous geostationary and polar orbiting observations, that corrections may be made to the Meteosat measurements so that they reproduce the Nimbus 7 ERB radiation budget values. We therefore intend to extend the studies described in this paper for different seasons and longer time periods in order to provide a more detailed statistical representation of the radiation budget for the European sector in order to provide the basis for a more accurate radiation climatology. Ultimately, this new, more accurate type of dataset from geostationary satellites could be obtained routinely, and could be used in conjunction with numerical forecasting models, such as those described by Geleyn (1982) and Slingo (1982).

Datasets produced from satellite data and archived over a long time period will be useful for monitoring changes in global cloudiness, producing statistics on cloudiness and as input and validation of global climate models. The incorporation of the right kind of global satellite data into medium range forecast models (Geleyn, 1982) may well help to improve their accuracy.

5. Acknowledgements

RWS was supported by a NERC grant for this work. The Meteosat data was supplied by ESOC, Darmstadt, FRG. The anisotropic scattering factors were supplied by Larry Stowe from NOAA/NESS, Washington D.C., who also gave many useful comments on this work. Helpful comments from Ken Bignell and Christopher England were also appreciated.

REFERENCES

Antikidis, P. and Reynolds, M. 1979. In-orbit calibration of Meteosat and its possible extension to other applications and fields. *ESA Journal 3*, 115–121.

Brooks, D. R. 1981. Grid systems for Earth radiation budget experiment applications. NASA Tech. Memo 83233.

Geleyn, J. F. 1982. Influence of the diurnal cycle on 10 day forecasting with the ECMWF global model. Symposium Über Strahlungstransport Probleme und Satellite Messungen in der Meteorologie und der Ozeanographie. Köln 22–26 March 1982, 27–29.

Gruber, A. and Winston, J. S. 1978. Earth-atmosphere radiative heating based on NOAA scanning radiometer measurements. *Bull. Am. Meteorol. Soc. 59*, 1570–1573.

Gube, M. 1980. Outgoing longwave flux computation from Meteosat data. *ESA Journal 4*, 381–396.

Gube, M. 1982. Planetary albedo estimates from Meteosat data. *ESA Journal 6*, 53–69.

Hickey, J. R., Stowe, L. L., Jacobowitz, H., Pellegrino, P., Maschoff, R. H., House, F. and Vonder Haar, T. H. 1980. Initial solar irradiance determinations from Nimbus 7 cavity radiometer measurements. *Science 208*, 281–283.

Hunt, G. E. 1982. On the sensitivity of a general circulation model climatology to changes in cloud structure and radiative properties. *Tellus 34*, 29–38.

Hunt, G. E. et al. 1983. The UCL Interactive Planetary Image Processing System (IPIPS) and its application to studies of planetary meteorology. *Trans IEEE*, submitted.

Jones, M. 1981. Navigation and deformation modelling for Meteosat imagery. *ESA Journal 5*, 287–304.

Kandel, R. and Bezanger, C. 1981. Diurnal variations of the infrared component of the Earth radiation budget. Presented at the International Radiation Symposium C.S.U. Aug. 11–16, 1980, Ft. Collins, Colorado, 387–389.

Knottenberg, H. and Raschke, E. 1982. On the discrimination of water and ice clouds in multispectral AVHRR data. Symposium Über Strahlungstransportprobleme und Satelliten Messungen in der Meteorologie und der Ozeanographie. Köln 22–26 March 1982, 145–147.

Köpke, P. 1980. Calibration of the Meteosat IR channel by ground measurements. *Contrib. Atmos. Phys. 53*, 442–445.

Kriebel, K. T. 1981. Calibration of the Meteosat VIS channel by airborne measurements. *Appl. Opt. 20*, 11–12.

Minnis, P. and Harrison, E. F. 1981. Diurnal variability of regional cloud radiative properties from geostationary satellite data. Presented at the 4th Conference on Atmospheric Radiation, Toronto, June 1981.

Morgan, J. 1980. Meteosat 1 calibration report. Issue 8, ESOC MDMD/MET.

Saunders, R. W. and Hunt, G. E. 1980. Meteosat observations of diurnal variation of radiation budget parameters. *Nature 283*, 645–647.

Saunders, R. W., Stowe, L. L. and Hunt, G. E. 1983. An intercomparison between radiation budget estimates from Meteosat 1, Nimbus 7 and Tiros-N satellites. *J. Appl. Meteorol.* (in press).

Slingo, J. M. 1982. A study of the Earth's radiation budget using a general circulation model. *Q. J. R. Meteorol. Soc. 108*, 379–406.

Smith, E. A. 1980. The modulation by tropical cloud systems of the bulk radiative heat budget. Presented at the International Radiation Symposium C.S.U. August 11–16, 1980, Fort Collins, Colorado, 352–354.

Stephens, G. L., Campbell, G. G. and Vonder Haar, T. H. 1981. Earth radiation budgets. *J. Geophys. Res. 86*, C10, 9739–9760.

Stowe, L. L., Jacobowitz, H. and Taylor, V. R. 1980. Reflectance characteristics of earth and cloud surfaces as measured by the ERB scanning channels on the Nimbus 7 satellite. Presented at the International Radiation Symposium C.S.U. August 11–16, Fort Collins, Colorado, 430–432.

Thekaekara, M. P. and Drummond, A. J. 1971. Standard values for the solar constant and its spectral components. *Nat. Phys. Sci. 229*, 6–9.

Vonder Haar, T. H. and Suomi, V. E. 1971. Measurements of the Earth's radiation budget from satellites during a five year period. Part 1: Extended time and space means. *J. Atmos. Sci. 28*, 305–314.

Ward, N. R., Saunders, R. W. and Hunt, G. E. 1983. Meteosat measurements of vertical fluxes in thunderstorms. *Int. J. Remote Sensing* (in press).